

REVISITING CALDERON'S PROBLEM

RAINALD LÖHNER AND HARBIR ANTIL

ABSTRACT. A finite element code for heat conduction, together with an adjoint solver and a suite of optimization tools was applied for the solution of Calderon's problem. One of the questions whose answer was sought was whether the solution to these problems is unique and obtainable. The results to date show that while the optimization procedure is able to obtain spatial distributions of the conductivity k that reduce the cost function significantly, the resulting conductivity k is still significantly different from the target distribution sought. While the normal fluxes recovered are very close to the prescribed ones, the tangential fluxes can differ considerably.

1. INTRODUCTION

The problem of trying to determine the material properties of a domain from boundary information is common to many fields. To mention just a few: mining (e.g. prospecting for oil and gas), medicine (e.g. trying to infer tissue properties), and engineering (e.g. trying to determine the existence and location of fissures).

From an abstract setting, it would seem that this is an ill-posed problem. After all, if we think of atoms, granules or some polygonal (e.g. finite element [FEM]) subdivision of space, the amount of data given resides in a space of one dimension less than the data sought. If we think of cuboid domain in d dimensions with N^d subdivisions, the amount of information/data given is of $O(N^{d-1})$ while the data sought is of $O(N^d)$.

Another aspect that would seem to indicate that this is an ill-posed problem is the possibility that many possible spatial distributions of material properties could yield very similar or equal boundary values. That this is indeed the case for some problems is shown below.

On the other hand, the propagation of physical properties (e.g. temperature, displacements, electrical currents, etc.) through the domain obeys physical conservation laws, i.e. some partial differential equations (PDEs). This implies that the material properties that can give rise to the data measured on the boundary are restricted by these conservation laws, i.e. are bounded. This would indicate that perhaps - due to these restrictions - the problem is not as ill-posed as initially thought.

2. CALDERON'S PROBLEM

In the following, we will consider conservation laws of the form:

2010 *Mathematics Subject Classification.* 35R30, 49N45, 65N21, 49K20, 49J20, 65N30.

Key words and phrases. Calderon Problem, Inverse Problems, Parameter Estimation, Optimization Problem, Heat Conduction, Finite Element Method.

The work of the second author is partially supported by NSF grants DMS-1818772 and DMS-1913004 and the Air Force Office of Scientific Research under Award NO: FA9550-19-1-0036.

$$\nabla \cdot \mathbf{f} = 0, \quad (2.1)$$

with

$$\mathbf{f} = k\nabla u, \quad (2.2)$$

implying

$$\nabla \cdot k\nabla u = 0, \quad \text{in } \Omega, \quad (2.3)$$

where u, k, \mathbf{f} denote the unknowns, material property and flux, and $\Omega \subset \mathbb{R}^d$, with $d \geq 1$ the domain considered with boundary Γ . For heat transfer problems, u is the temperature, k the conductivity, \mathbf{f} the heat flux, and (2.2) Fourier's law. For electrical currents, u is the voltage, k the resistivity, \mathbf{f} the electrical current, and (2.2) Ohm's law.

Eqn. (2.3) needs appropriate boundary conditions in order to be uniquely solvable. On the boundary Γ we can prescribe u (Dirichlet), $f_n = \mathbf{n} \cdot \mathbf{f}$ (Neumann) or a combination of both (Robin), i.e.

$$\alpha u + \beta f_n = b, \quad \text{on } \Gamma, \quad (2.4)$$

Calderon's problem [4] may then be formulated as follows:

- Given a PDE of the form of (2.3);
- Given **both** u and f_n on Γ ;
- Determine $k(\mathbf{x})$ in Ω .

Ever since Calderon first formulated this problem in 1980 [4], several proofs of existence, uniqueness and solvability have been given [1, 2, 3, 8]. However, as will be seen, the problem remains difficult. It is also interesting to observe that there is apparently no 'canonical test problem' or 'canonical test suite of problems' for this class of problems. This is in sharp contrast to other engineering disciplines such as aerodynamics, hydrodynamics and electromagnetics, where standard test problems have evolved over the years.

3. THE 1-D CASE

In 1-D, (2.1)-(2.3) reduce to:

$$f = f_c, \quad k \frac{du}{dx} = f_c, \quad (3.1)$$

where f_c is the constant heat flux. This implies that only one measurement point is required for f_n (note also: in 1-D $f_n = f$). Given a domain $0 \leq x \leq L$ and $k > 0$, we can integrate

$$\frac{du}{dx} = \frac{f_c}{k}, \quad (3.2)$$

implying

$$u(L) - u(0) = f_c \int_0^L \frac{1}{k} dx, \quad (3.3)$$

or:

$$\int_0^L \frac{1}{k} dx = \frac{u(L) - u(0)}{f_c}. \quad (3.4)$$

Calderon's problem in 1-D then reduces to determining k given $u(0), u(L)$, and f_c . This is unique for constant $k(x) = k_c$, but not for arbitrary distributions of $k(x)$. If we consider n regions Δx_i , $i = 1, \dots, n$ with different k_i , then all that is required is:

$$\sum_{i=1}^n \frac{\Delta x_i}{k_i} = \frac{u(L) - u(0)}{f_c}, \quad (3.5)$$

which clearly allows for infinitely many possible solutions. To illustrate this, consider the simple case with: $L = 1, u(0) = 1, u(1) = 0, f_c = -1$. Assuming 4 equal regions of $\Delta x = 0.25$, (3.5) implies:

$$\sum_{i=1}^4 \frac{1}{k_i} = 4, \quad (3.6)$$

which may be realized, e.g. via

- a) $k_1 = k_2 = k_3 = k_4 = 1$;
- b) $k_1 = k_2 = 2; k_3 = k_4 = 2/3$;
- c) $k_1 = 10, k_2 = 5, k_3 = 2, k_4 = 10/32$;
- d) ...

Moreover, the spatial sequence of k 's can be changed without affecting the resulting flux, so that even highly oscillatory distributions of k are admissible. Four of these possibilities have been plotted in Figure 1 (a), (b) and Figure 2 (c), (d).

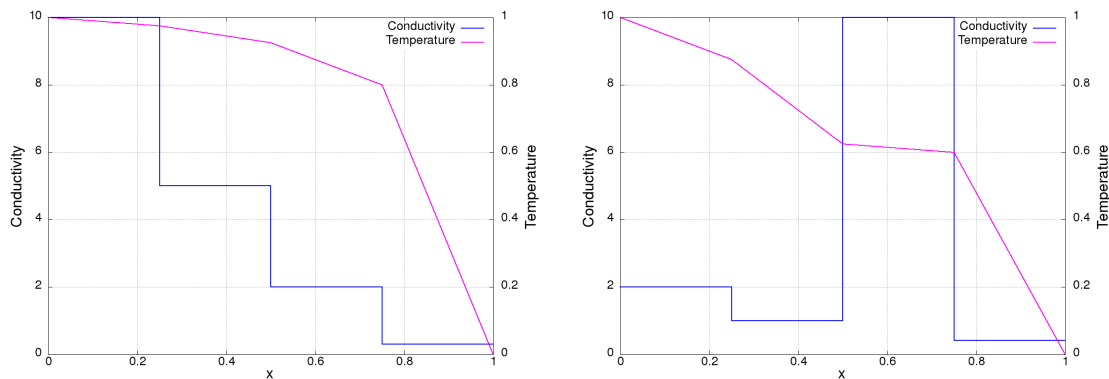


FIGURE 1. 1D Case (a), (b): Possible Conductivities and Resulting Temperatures for $f_c = -1$.

Why would Calderon's problem then be easier to solve or perhaps uniquely solvable in higher dimensions? Consider again the 1-D case, and assume that this is a bar/hexahedral domain with equal material properties along the y, z directions, as well as Neumann boundary conditions at the y, z boundaries. In the 1-D case, we have restricted the data input to only 3 items: a constant temperature for planes $x = 0, x = L$, and the heat flux at $x = 0$. In the 3-D case, we could measure the temperature and fluxes at all boundaries (and in particular the y, z boundaries along the x axis, and we could impose a temperature that is not constant in y, z for the planes $x = 0, x = L$. This would yield much more information than in the 1-D case, and may lead to a solvable problem.

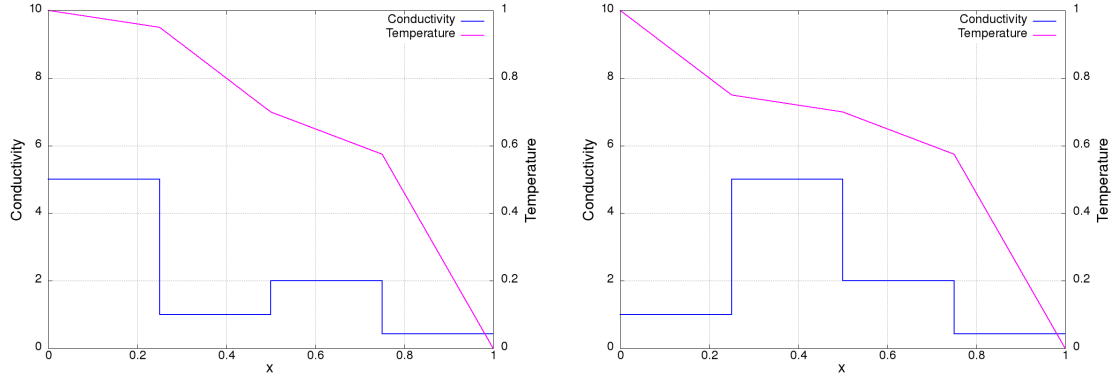


FIGURE 2. 1D Case (c), (d): Possible Conductivities and Resulting Temperatures for $f_c = -1$.

On the other hand, one may encounter difficulties for the multidimensional cases when regions with $\nabla u \approx 0$ are present. In these cases it is irrelevant which value of k is used, as the flux is vanishingly small anyhow. As an example, consider the 2-D case $0 \leq x \leq 3$, $0 \leq y \leq 1$ shown in Figure 3. The domain is divided into 3 regions and the conductivity in these three regions is set to $k_{left} = 1.0$, $k_{middle} = 10.1$, $k_{right} = 1.0$. The value of u on the boundary was set to $u|_{\Gamma} = 0$, except for $x \leq 1$ where $u|_{\Gamma} = (y - 0.5)(x - 1)^2$. As one can see from the temperature and the fluxes, in the right part of the domain very small gradients of u are obtained. This would indicate that one has to be careful when ‘conducting a measurement’, imposing values of u , f_n that yield useful information about the spatial distribution of k .

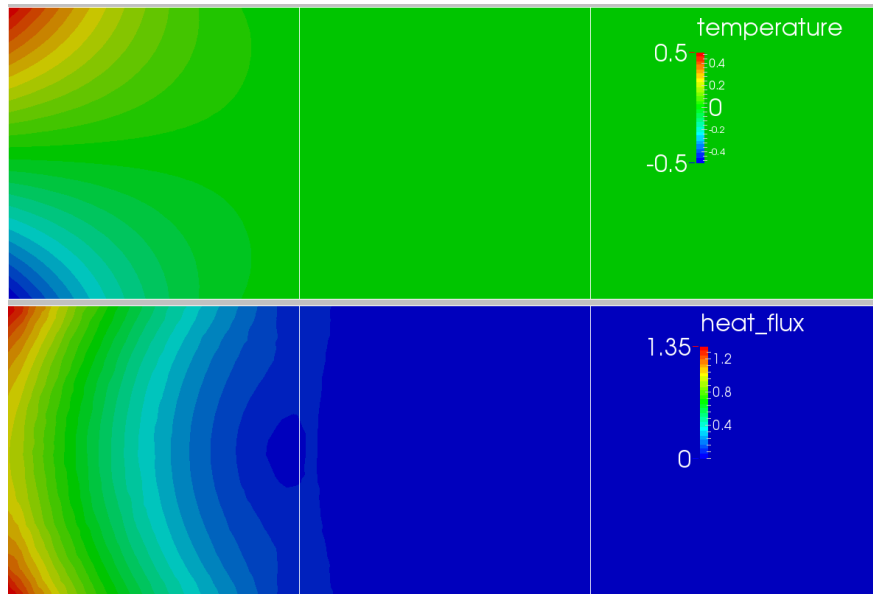


FIGURE 3. 2D Case With Small Values for ∇u .

4. CALDERON'S PROBLEM AND OPTIMIZATION

Calderon's problem may be formulated as an optimization problem with PDE constraints for $k(\mathbf{x})$ as follows: Given m measurements with data $\{(u_m, f_m)\}_m$ on the boundary, minimize the cost functional:

$$I(u_m, k) = \frac{1}{2} \sum_m \int_{\Gamma} (f_m - k \mathbf{n} \cdot \nabla u_m)^2 d\Gamma, \quad (4.1)$$

subject to PDE constraints

$$R(u_m, k) = \nabla \cdot k \nabla u_m = 0, \quad \text{in } \Omega \quad (4.2)$$

with boundary condition

$$u_m = u_m^0, \quad \text{on } \Gamma. \quad (4.3)$$

In the most general case, one may consider a spatial subdivision of space (e.g. a FEM discretization) and functions with local support so that:

$$k(\mathbf{x}) = \sum_i N^i(\mathbf{x}) \hat{k}_i,$$

where $N^i(\mathbf{x})$ are known functions (e.g. FEM shape functions) and \hat{k}_i the discrete values (i.e. degrees of freedom, design parameters) sought. At the core of any optimization tool is the cost function evaluation. In the present case, this implies invoking a field solver m times for (4.2), in the weak form, followed by boundary evaluation for (4.1). As we are seeking domain information, the number of design variables may be very large. This implies that non-gradient based procedures (e.g. genetic algorithms), or finite difference based gradient techniques may be prohibitively expensive.

5. OPTIMIZATION VIA ADJOINTS

The purpose of this section is to use the formal Lagrangian approach to derive the necessary optimality conditions for (4.1)-(4.3). The cost functional can be extended to the Lagrangian functional

$$L(u_m, k, \tilde{u}_m, \tilde{v}_m) = I(u_m, k) - \sum_m \int_{\Omega} \tilde{u}_m \nabla \cdot k \nabla u_m d\Omega + \sum_m \int_{\Gamma} \tilde{v}_m (u_m - u_m^0) d\Gamma, \quad (5.1)$$

where \tilde{u}_m, \tilde{v}_m are the Lagrange multipliers (adjoints) corresponding to the state equation (4.2) and the boundary condition (4.3), respectively. Repeated integration by parts leads to:

$$\begin{aligned} L(u_m, k, \tilde{u}_m, \tilde{v}_m) &= I(u_m, k) + \sum_m \int_{\Omega} k \nabla \tilde{u}_m \nabla u_m d\Omega \\ &\quad - \sum_m \int_{\Gamma} \tilde{u}_m k \mathbf{n} \cdot \nabla u_m d\Gamma + \sum_m \int_{\Gamma} \tilde{v}_m (u_m - u_m^0) d\Gamma, \end{aligned} \quad (5.2)$$

$$\begin{aligned} L(u_m, k, \tilde{u}_m, \tilde{v}_m) &= I(u_m, k) - \sum_m \int_{\Omega} u_m \nabla \cdot k \nabla \tilde{u}_m d\Omega + \sum_m \int_{\Gamma} u_m k \mathbf{n} \cdot \nabla \tilde{u}_m d\Gamma \\ &\quad - \sum_m \int_{\Gamma} \tilde{u}_m k \mathbf{n} \cdot \nabla u_m d\Gamma + \sum_m \int_{\Gamma} \tilde{v}_m (u_m - u_m^0) d\Gamma. \end{aligned}$$

Considering a variation with respect to u_m in a direction h results in:

$$D_{u_m}L(u_m, k, \tilde{u}_m, \tilde{v}_m)h = - \int_{\Gamma} [(f_m - k \mathbf{n} \cdot \nabla u_m)k \mathbf{n} \cdot \nabla h - hk \mathbf{n} \cdot \nabla \tilde{u}_m + \tilde{u}_m k \mathbf{n} \cdot \nabla h - h\tilde{v}_m] d\Gamma - \int_{\Omega} h \nabla \cdot k \nabla \tilde{u}_m d\Omega = 0.$$

Selecting h so that h and all its derivatives are zero on Γ yields the *adjoint equation* in the domain Ω :

$$\nabla \cdot k \nabla \tilde{u}_m = 0. \quad (5.3)$$

Choosing h such that $h = 0$ on Γ but $k \mathbf{n} \cdot \nabla h \neq 0$ yields the boundary conditions for \tilde{u}_m :

$$\tilde{u}_m = - (f_m - k \mathbf{n} \cdot \nabla u_m). \quad (5.4)$$

Notice that by letting $h \neq 0$ on Γ gives a compatibility condition between \tilde{v}_m and \tilde{u}_m . Finally, performing a variation of L , in (5.2), with respect to k in a direction h leads to:

$$D_k L(u_m, k, \tilde{u}_m, \tilde{v}_m)h = \sum_m \left[\int_{\Gamma} - (f_m - k \mathbf{n} \cdot \nabla u_m) \mathbf{n} \cdot \nabla u_m h d\Gamma + \int_{\Omega} h \nabla u_m \cdot \nabla \tilde{u}_m d\Omega - \int_{\Gamma} \tilde{u}_m \mathbf{n} \cdot \nabla u_m h d\Gamma \right], \quad (5.5)$$

which, after using (5.4), is equivalent to:

$$D_k L(u_m, k, \tilde{u}_m, \tilde{v}_m)h = \sum_m \left[\int_{\Omega} \nabla u_m \cdot \nabla \tilde{u}_m h d\Omega \right]. \quad (5.6)$$

The consequences of this rearrangement are profound:

- The gradient of L , I (cf. 5.6) with respect to k may be obtained by solving m forward (4.2)-(4.3) and adjoint (5.3)-(5.4) problems; i.e.
- The cost for the evaluation of gradients in (5.6) is **independent of the number of variables used for k** (!). This implies that the material coefficients k sought may be described by a very large parameter set (for example a constant value for each Finite Element), something that would be computationally prohibitively expensive for methods that obtain gradients via finite differences of the objective function.

A gradient descent based optimization cycle using the adjoint approach is then composed of the following steps:

- For each measurement m :
 - With current k : solve (4.2)-(4.3) for the field variable $\rightarrow u_m$
 - With current k and u_m : solve (5.3)-(5.4) for the adjoint field variable $\rightarrow \tilde{u}_m$
 - With u_m, \tilde{u}_m : obtain gradients for each $m \rightarrow I(u_m)_{,k}$
- Sum up the gradients $\rightarrow I_{,k} = \sum_m I(u_m)_{,k}$
- Smooth gradients (regularization) $\rightarrow I_{,k}^s$
- Update $k_{new} = k_{old} - \alpha I_{,k}^s$, where α is the step-length.

Here and subsequently $I_{,k} := \partial I / \partial k$.

6. SMOOTHING OF GRADIENTS

The gradients of the cost function with respect to k allow for oscillatory solutions. One must therefore smooth or ‘regularize’ the spatial distribution. This happens naturally when using few degrees of freedom, i.e. when k is defined via other spatial shape functions (e.g. larger spatial regions of piecewise constant k). As the (possibly oscillatory) gradients obtained in the (many) finite elements are averaged over spatial regions, an intrinsic smoothing occurs. This is not the case if k and the gradient are defined and evaluated in each element separately, allowing for the largest degrees of freedom in a mesh and hence the most accurate representation. Three different types of smoothing or ‘regularization’ were considered. All of them start by performing a volume averaging from elements to points:

$$\hat{k}_i = \frac{\sum_{el} \hat{k}_{el} V_{el}}{\sum_{el} V_{el}}, \quad (6.1)$$

where $\hat{k}_i, \hat{k}_{el}, V_{el}$ denote the value of k at point i , as well as the values of k in element el and the volume of element el , and the sum over all the elements surrounding point i .

6.1. Simple Point/Element/Point Averaging. In this case, the values of k are cycled between elements and points. When going from point values to element values, a simple average is taken:

$$\hat{k}_{el} = \frac{1}{n_{el}} \sum_i \hat{k}_i, \quad (6.2)$$

where n_{el} denotes the number of nodes (degrees of freedom) of an element and the sum extends over all the nodes of the element. After obtaining the new element values via (6.2) the point averages are again evaluated via (6.1). This form of averaging is very crude, but works surprisingly well.

6.2. H^1 (Weak) Laplacian Smoothing. In this case, the initial values k_0 obtained for k are smoothed via:

$$[1 - \lambda_l \nabla^2] k = k_0. \quad (6.3)$$

Here λ is a free parameter which may be problem and mesh dependent (its dimensional value is length squared). Discretization (of the weak form of (6.3)) via FEM yields:

$$[\mathbf{M}_c + \lambda_l \mathbf{K}] \mathbf{k} = \mathbf{M}_c \mathbf{k}_0, \quad (6.4)$$

where \mathbf{M}_c, \mathbf{K} denote the consistent mass matrix and the stiffness matrix obtained for the Laplacian operator.

6.3. H^1 (Weak) Pseudo-Laplacian Smoothing. One can avoid the dimensional dependency of λ in (6.3) by smoothing via:

$$[1 - \lambda_{pl} \nabla \cdot h_{fem}^2 \nabla] k = k_0, \quad (6.5)$$

where h_{fem} is a characteristic element size (e.g. average of element sides, average of element normals, or any other sensible measure of element size). For linear elements, one can show that this is equivalent to:

$$[\mathbf{M}_c + \lambda_{pl} (\mathbf{M}_l - \mathbf{M}_c)] \mathbf{k} = \mathbf{M}_c \mathbf{k}_0, \quad (6.6)$$

where \mathbf{M}_l denotes the lumped mass matrix [14]. In the examples shown below this form of smoothing was used for the gradients, setting $\lambda_{pl} = 0.05$.

6.4. Relaxation. As the main aim of the smoothing given by (6.3)-(6.6) is the removal of high frequency modes, simple relaxation procedures that do not require the inversion of a large matrix offer an effective way to proceed. Eqns. (6.4), (6.6) may be recast as:

$$\mathbf{L}\mathbf{u} = \mathbf{r}.$$

This may be interpreted as the steady result of the following transient problem:

$$\mathbf{C}\mathbf{u}_{,\tau} + \mathbf{L}\mathbf{u} = \mathbf{r}.$$

where τ denotes a pseudo-time and \mathbf{C} contains the diagonal entries of \mathbf{L} . This is solved via explicit integration:

$$\mathbf{C}(\mathbf{u}^{n+1} - \mathbf{u}^n) = \delta\tau(\mathbf{r} - \mathbf{L}\mathbf{u}^n).$$

A value of $\delta\tau = 0.8$ was set for all numerical examples in the next section. It was observed that the number of explicit steps required for effective smoothing is of the order of 10. For 3-D cases, it is far more economical to use such a relaxation procedure than inverting the matrix \mathbf{L} .

6.5. Gradient Projection. Intrigued by some of the results obtained, and in order to check whether the gradients obtained via the adjoint method were correctly computed, the option of projecting the gradients to a region discretization of k based on volumes V_i^{reg} with constant k was implemented. Given the discretization:

$$I_{,k}(\mathbf{x}) \approx \sum_i H_i \left(\hat{I}^{reg,k} \right)_i,$$

where

$$H_i(\mathbf{x}) = \begin{cases} 1 & \forall \mathbf{x} \in V_i^{reg}, \\ 0 & \forall \mathbf{x} \notin V_i^{reg}. \end{cases}$$

and $(\hat{I}^{reg,k})_i$ denote the (constant) values of the gradient of I with respect to k in region V_i^{reg} , and given $I_{,k}(\mathbf{x})$ from the (fine) FEM mesh, the gradient is averaged over each volume as:

$$\left(\hat{I}^{reg,k} \right)_i = \frac{\int_{V_i^{reg}} I_{,k}(\mathbf{x}) dV}{\int_{V_i^{reg}} dV}.$$

This gradient is then passed back to gradient-based optimizers to continue the iteration towards the minimum of the cost function.

7. EXAMPLES

All the numerical examples are carried out using FEHEAT, a finite element code based on simple linear (beam), triangular (plate) and tetrahedral (volume) elements with constant conductivity per element. The optimization loops are steered via a user-defined cost function and FEOPT, a general optimization code, for the finite difference gradient-based optimization, or via a simple shell-script for the adjoint-based optimization. In all cases, a ‘target’ distribution of $k(\mathbf{x})$ and u_Γ is generated with user-defined subroutines. The forward problem is then solved, i.e. $u(\mathbf{x})$ and $\mathbf{f}(\mathbf{x})$ are obtained. This then yields the ‘measurement data’

u_Γ, f_Γ that is used for the Calderon's problem. A series of tests are conducted to see if the conductivities obtained by the optimization algorithm are dependent on the initial spatial distribution of the conductivity. The results showed no influence (all cases converged to the same solution). Therefore, all optimization cases are started from a constant $k(\mathbf{x}) = k_0$, and the convergence to the 'target' distribution of $k(\mathbf{x})$, by minimizing the error with respect to the 'measured flux' given by (4.1), is observed. As stated in the introduction, it is possible that many different spatial distributions of $k(\mathbf{x})$ could minimize the error measure given by (4.1).

As it appears that no 'canonical test problem' or 'canonical test suite of problems' for this class of problems exists, an attempt has been made to start from simple cases and then proceed to more difficult ones.

7.1. Square. This case is a 2-D case, but was run in 3-D. The domain and spatial discretization are shown in Figure 4. The dimensions are $0 \leq x \leq 1, 0 \leq y \leq 1, 0 \leq z \leq 0.05$. This case was run repeatedly, increasing the level of complexity and measurements. The base mesh had elements of size approximately $h = 0.025$ (the ideal tetrahedron is not a space-filling element), which led to 12,461 elements and 3,347 points. The cases were also run on coarser meshes and no significant difference in results or convergence behavior was observed.

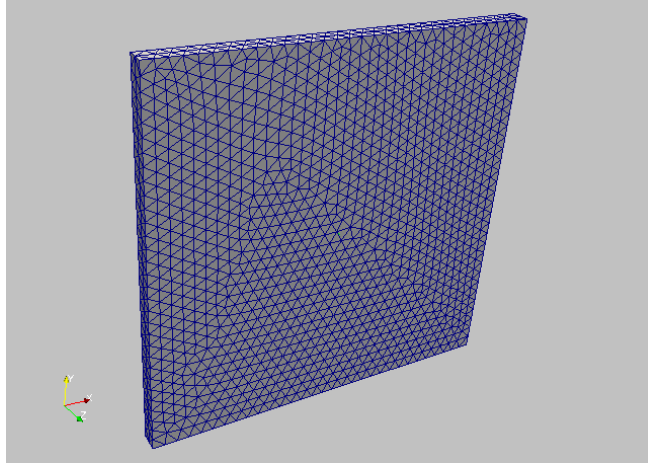


FIGURE 4. Square: FEM Mesh Used.

7.1.1 Constant k

For this first test the desired (or target) conductivity k is set to $k(\mathbf{x}) = 2$. The temperature is set in a way that is similar to the application of electric potentials in Electrical Impedance Tomography [11, 13, 5, 12, 6, 9, 10, 7] via a set of 'hot' and 'cold' 'sources' and 'sinks' of the form:

$$u(\mathbf{x}) = \sum_i S_i(\mathbf{x}, \mathbf{x}_i, r_i, a_i),$$

with

$$S_i(\mathbf{x}, \mathbf{x}_i, r_i, a_i) = a_i e^{-\frac{(\mathbf{x}-\mathbf{x}_i)^2}{r_i^2}}.$$

One source and one sink is used for each ‘measurement’ as follows:

- First ‘Measurement’ Parameters:
 - $S_1 : \mathbf{x}_1 = (0.5, 0.0)$, $r_1 = 0.5$, $a_1 = 1.0$
 - $S_2 : \mathbf{x}_2 = (0.5, 1.0)$, $r_2 = 0.5$, $a_2 = -1.0$
- Second ‘Measurement’ Parameters:
 - $S_1 : \mathbf{x}_1 = (0.0, 0.5)$, $r_1 = 0.5$, $a_1 = 1.0$
 - $S_2 : \mathbf{x}_2 = (1.0, 0.5)$, $r_2 = 0.5$, $a_2 = -1.0$

The case is first run with one and then with two measurements. Figures 5 (a), (b) show the target temperature field and fluxes field obtained after 10 steps (at this point the conductivity is very close to the target conductivity and the difference in temperature and fluxes between step 10 and subsequent steps negligible). The errors measured for the fluxes, as well as the L2 error of the conductivity are shown in Figures 6 (left) and (right), respectively. Noticeable in this result is the much faster rate of convergence when two measurements are used.

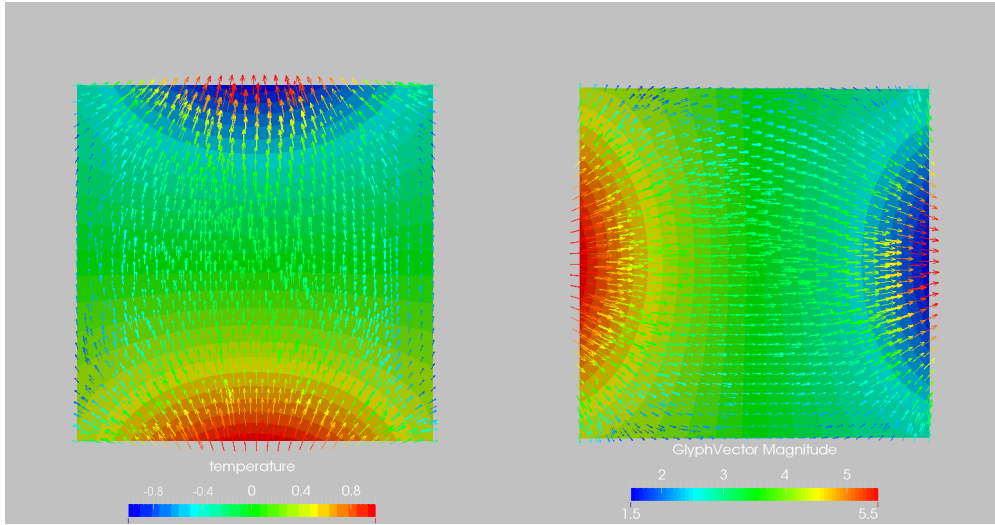


FIGURE 5. Square (a), (b) - constant k : Temperatures and Fluxes for Measurements 1,2.

7.1.2 Linear k

The next test considers as a target a linear conductivity of the form:

$$k(\mathbf{x}) = 2 - x .$$

The up to four temperature fields prescribed (i.e. measurements) are shown in Figure 7. The conductivity k in each element was set constant, based on the element centroid (average of the 4 nodes). Figures 8 show the target conductivity (left) and the conductivity obtained with four measurements (right). Note that because the graphics first average to point values and then perform the plane cut for display even the target (exact) conductivity appears noisy. Nevertheless, a difference between the target and recovered conductivity may be observed. The errors measured for the fluxes, as well as the L2 error of the conductivity are shown in Figures 9 (left) and (right), respectively. As before, a single measurement seems to

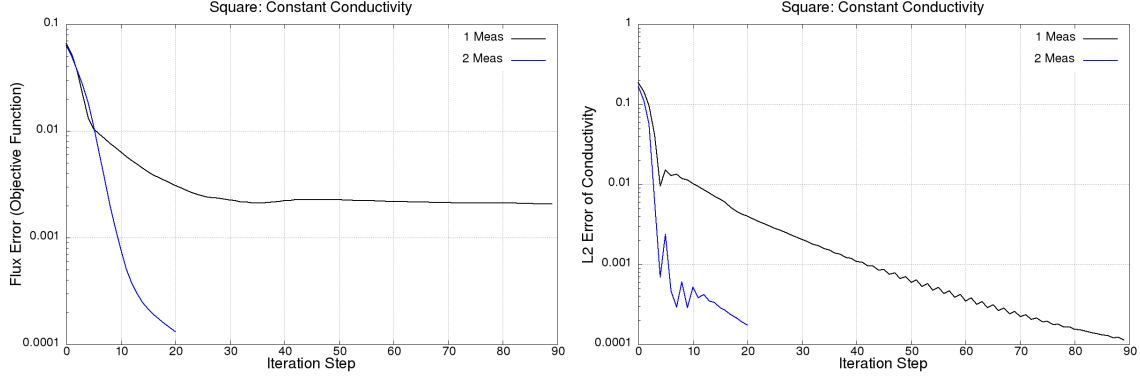


FIGURE 6. Square - constant k : Errors in Fluxes (left) and Conductivity (right).

lead to slower convergence. It also appears that the number of measurements at some point ‘saturates’: 4 measurements do not yield a better or faster result than 2 measurements.

7.1.3 Gaussian k

In this case the target distribution for k is given by:

$$k(\mathbf{x}) = 1 + 4e^{\left(\frac{|\mathbf{x}-\mathbf{x}_0|}{r_0}\right)^2}, \quad \mathbf{x}_0 = (0.5, 0.5, 0.025), \quad r_0 = 0.2.$$

The same 4 ‘measurement functions’ as before are used for this case. For the optimization via finite differences, the distribution of k was given by constant regions spaced in a cartesian lattice in x, y . Figures 10, 11, 12 show the results obtained using 25 and 49 degrees of freedom for the finite difference gradient and projected adjoint gradient optimization, as well as the adjoint. The decrease in objective function for these cases is shown in Figure 13 (left), and the L2 error of the conductivity in Figure 13 (right). Note that the optimization procedure as such works, recovering well the specified normal flux distribution on the boundary. Note the slow convergence of the adjoint, which may be attributable to the much larger degrees of freedom. Note also that the spatial distribution for k , while resembling the target distribution, still has considerable differences. Seemingly, the lower the degrees of freedom, the better the result (!).

7.1.4 Disk-Like k

Intrigued by the previous result, a case with very few design parameters has been chosen. The (discontinuous) target distribution for k of the form:

$$k(\mathbf{x}) = k_{disk} = 5 \quad \forall |\mathbf{x} - \mathbf{x}_0| \leq r_0, \quad k(\mathbf{x}) = k_{exte} = 1 \quad \forall |\mathbf{x} - \mathbf{x}_0| > r_0, \\ \mathbf{x}_0 = (0.5, 0.5, 0.025), \quad r_0 = 0.25.$$

Two ‘measurement functions’ were used for this case. The case was run with only 4 design parameters: x_0, y_0, r_0 and k_{disc} . The initial values were set to: $x_0 = y_0 = 0.25, r_0 = 0.1, k_{disc} = 2$, i.e. relatively far away from the target parameters. The results obtained are shown in Figures 14, 15, 16. The decrease in objective function for these cases is shown in Figure 17 (left), and the L2 error of the conductivity in Figure 17 (right). Note the fast convergence and the correct position for the target conductivity. The radius obtained is a bit larger, which implies that the conductivity obtained k_{disk} has to be lower. However, the

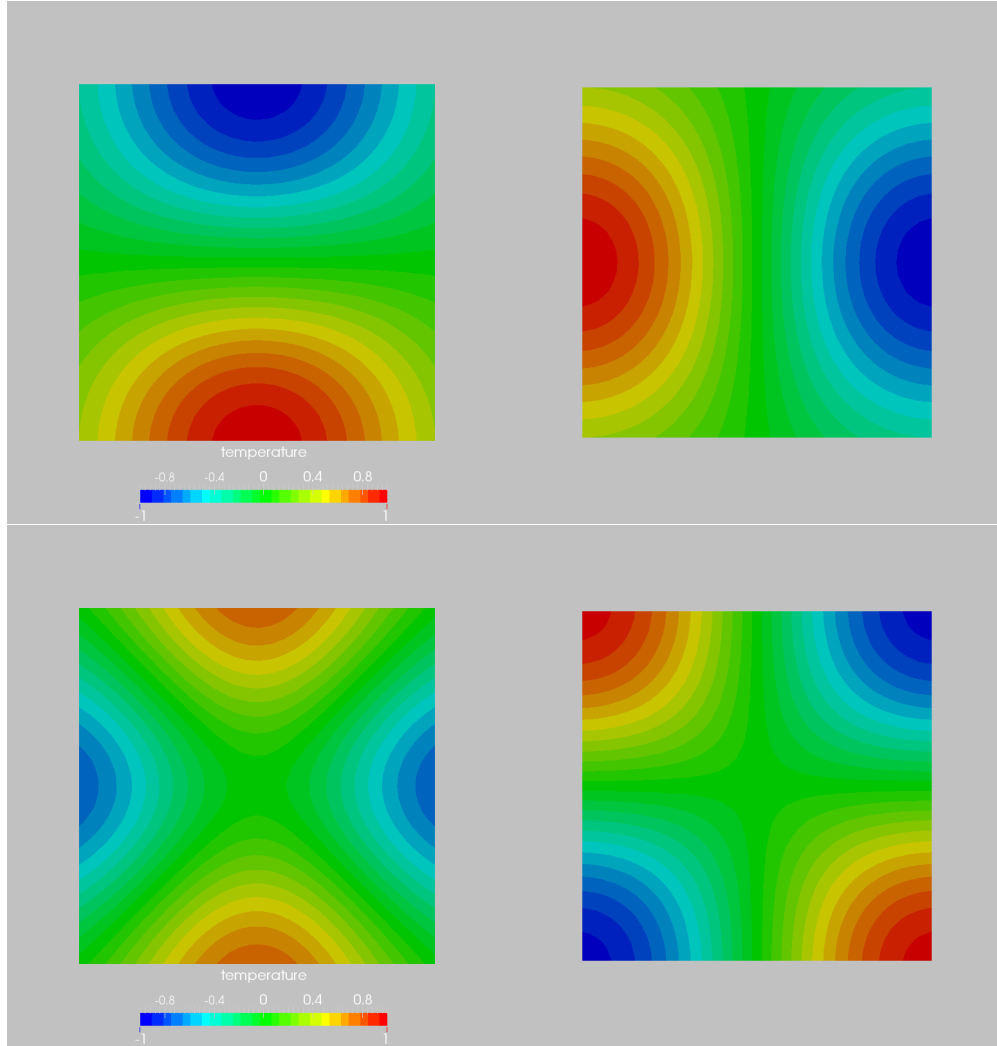


FIGURE 7. Square - linear k : Temperatures for Measurements 1-4.

normal boundary fluxes are indistinguishable from one another (see Figure 16). We remark that the optimizer has converged to a relative design parameter range of $\epsilon_r = 10^{-3}$, i.e. both r_0 and k_{disk} will not change significantly even if ϵ_r is set lower.

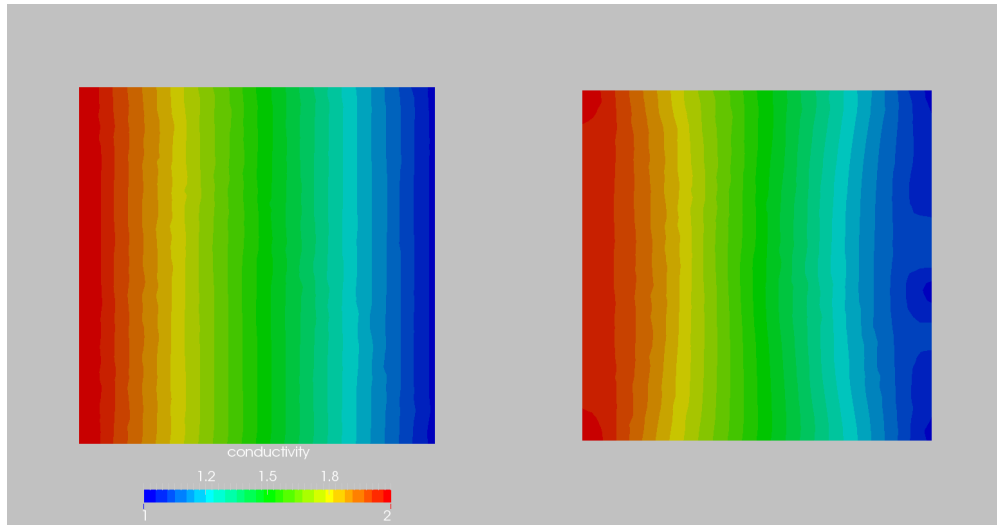


FIGURE 8. Square - linear k : Target (Left) and Recovered (Right) Conductivity with 4 Measurements.

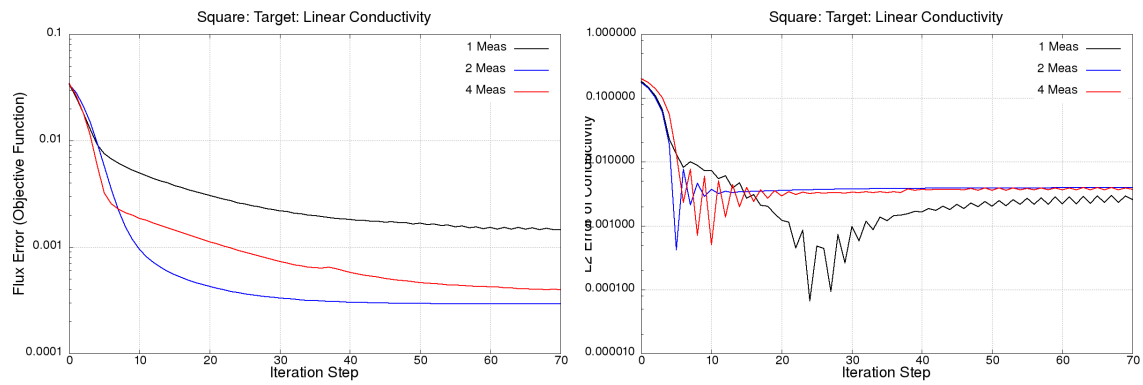


FIGURE 9. Square - linear k : Errors in Fluxes (left) and Conductivity (right).

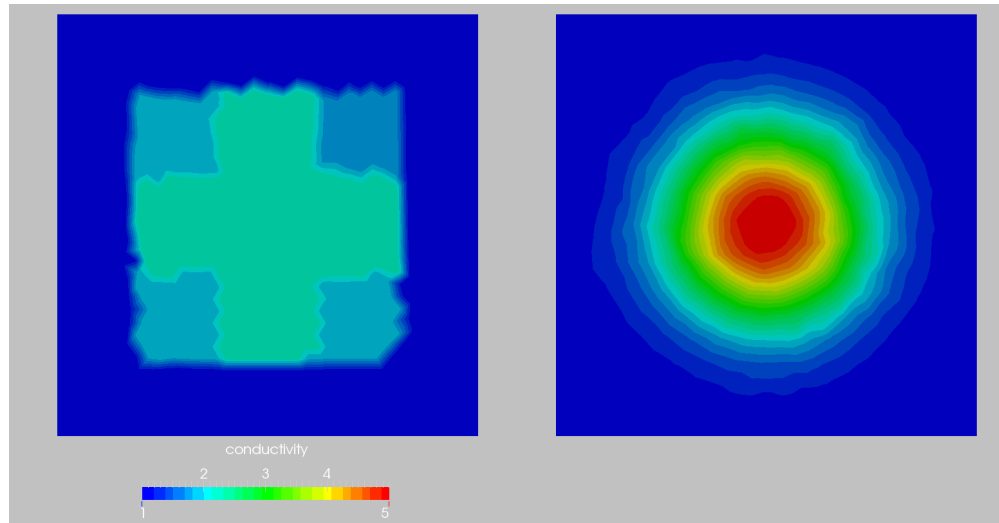


FIGURE 10. Square - Gaussian k : Conductivity Distribution: Left: 25 DOFs, Right: Target.

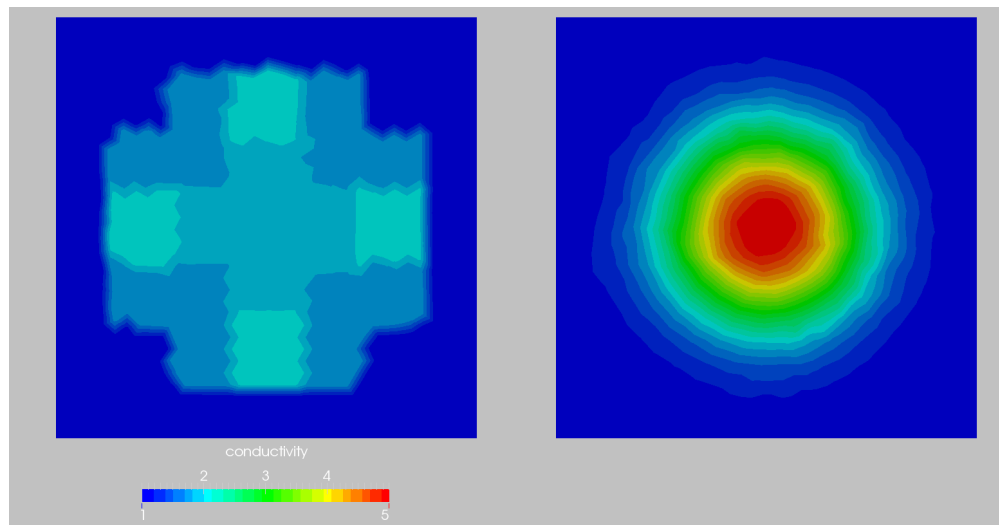


FIGURE 11. Square - Gaussian k : Conductivity Distribution: Left: 49 DOFs, Right: Target.

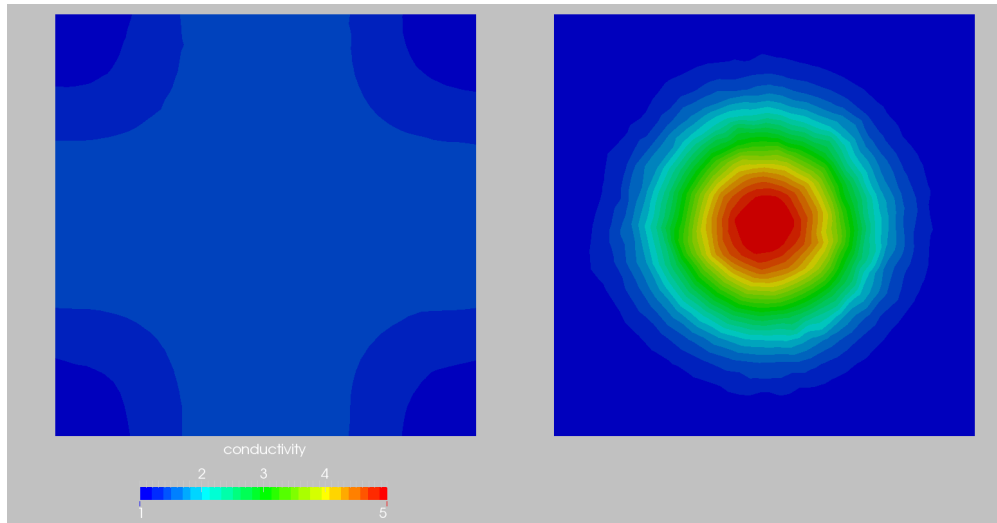


FIGURE 12. Square - Gaussian k : Conductivity Distribution: Left: Adjoint-Based, Right: Target.

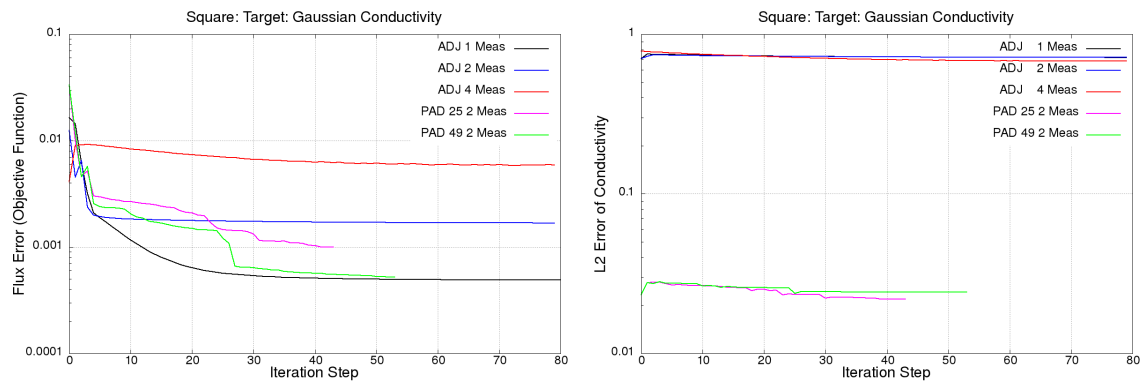


FIGURE 13. Square - Gaussian k : Errors in Fluxes (left) and Conductivity (right).

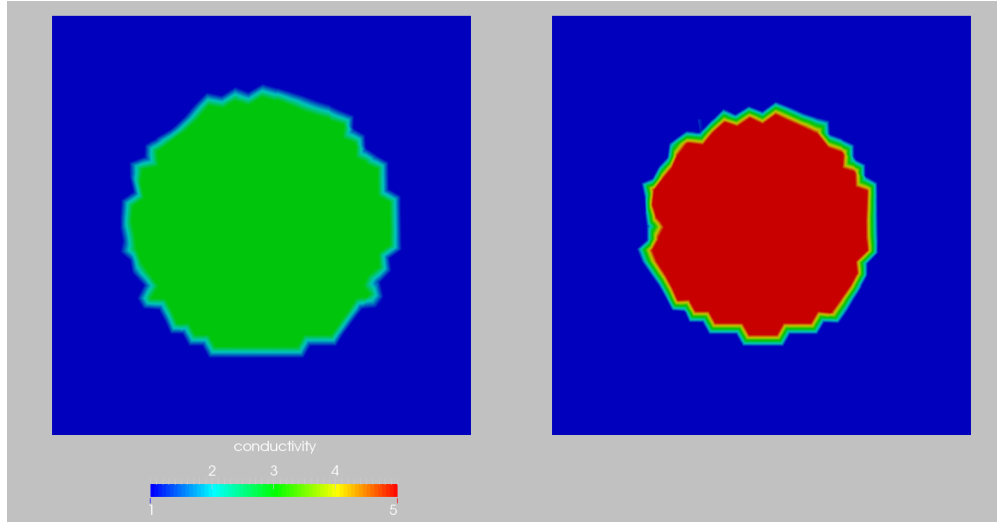


FIGURE 14. Square - Disk-Like k : Conductivity Distribution: Left: Converged Result, Right: Target

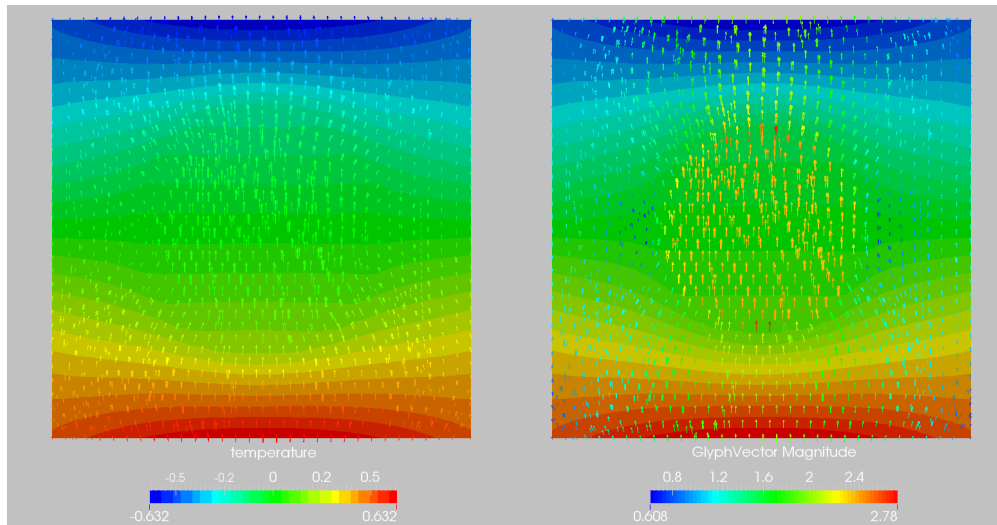


FIGURE 15. Square - Disk-Like k : Temperature and Flux Distribution: Left: Converged Result, Right: Target

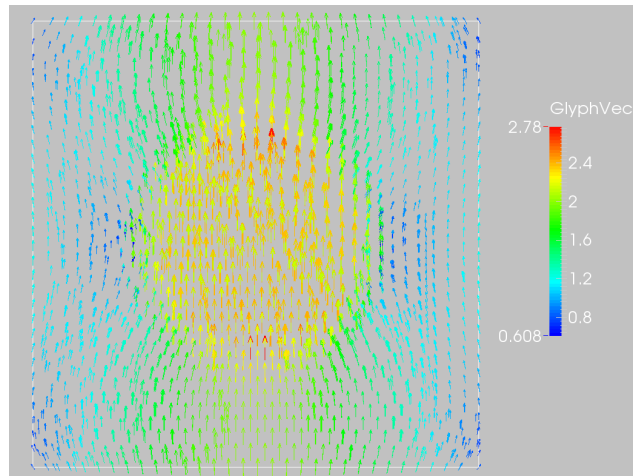


FIGURE 16. Square - Disk-Like k : Comparison of Flux Distribution for Converged Result and Target

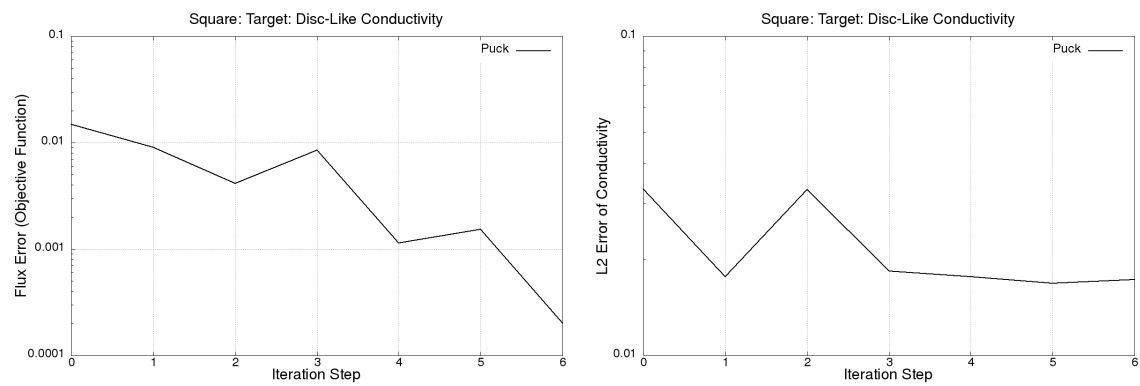


FIGURE 17. Square - Disk-Like k : Errors in Fluxes (left) and Conductivity (right)

7.2. **Cube.** This case is similar to the one shown before, but fully 3-D. The domain dimensions are $0 \leq x \leq 1, 0 \leq y \leq 1, 0 \leq z \leq 1$. The finite element mesh had more than 250,000 tetrahedral elements of uniform size.

7.2.1 Gaussian k

In this case the target distribution for k is given by:

$$k(\mathbf{x}) = 1 + 4e^{\left(\frac{|\mathbf{x}-\mathbf{x}_0|}{r_0}\right)^2} \quad \mathbf{x}_0 = (0.5, 0.5, 0.05) \quad r_0 = 0.2.$$

Three measurement functions similar to the ones used before were placed at the center of each face so as to induce a heat flux that is mainly directed in the x, y, z -directions respectively. For the optimization via finite differences, the distribution of k was given by constant regions spaced in a cartesian lattice in x, y, z . Figures 18-24 show the results obtained using 125 degrees of freedom for the finite difference gradient and the more than 250,000 degrees of freedom when using each element conductivity. Figure 25 depicts the comparison of fluxes for plane $y = 0$. One can see that the optimization procedure as such works, recovering well the specified normal flux distribution on the boundary, even though the spatial distribution for k is very different from the target. As before, apparently the lower the degrees of freedom, the better the result (!). The decrease in objective function for these cases is shown in Figure 26 (left), and the L2 error of the conductivity in Figure 26 (right).

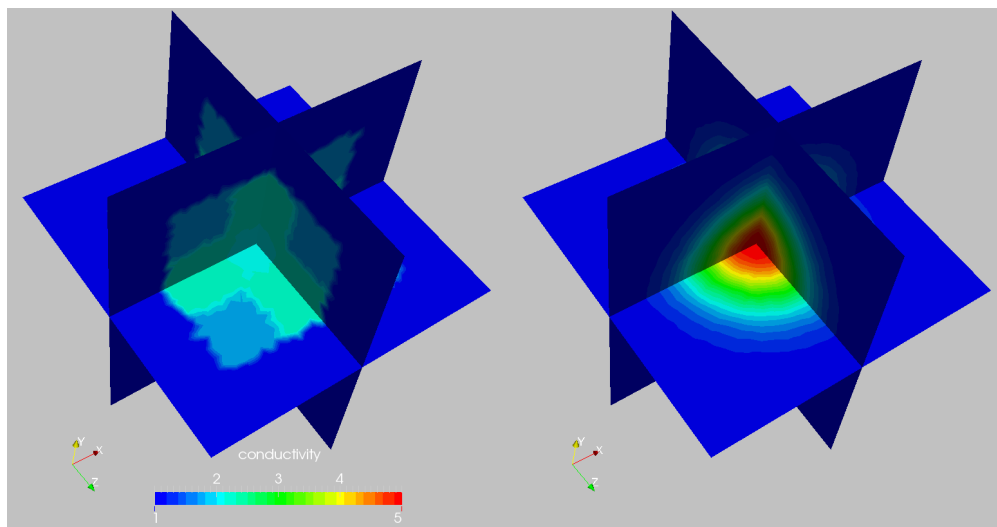


FIGURE 18. Cube - Gaussian k : Conductivity Distribution: Left: 125 DOFs, Right: Target

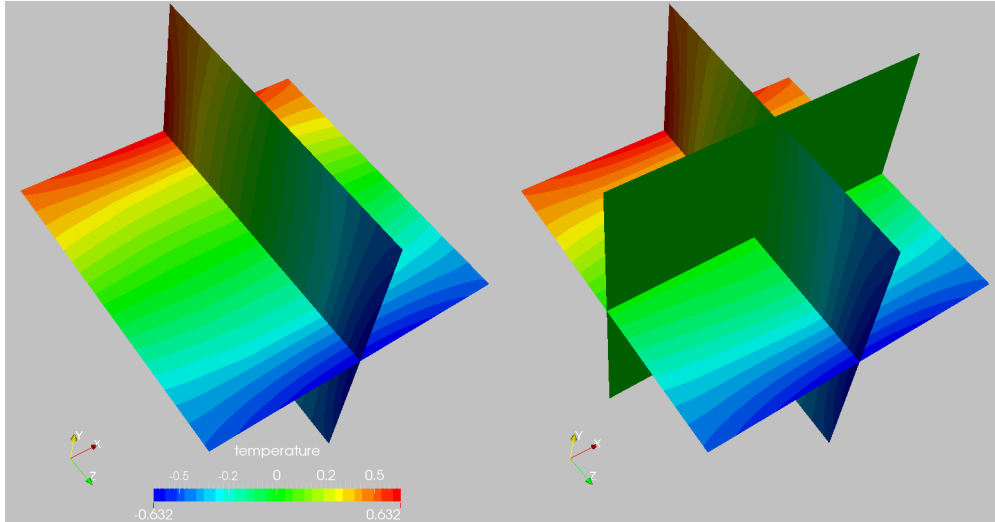


FIGURE 19. Cube - Gaussian k : Temperature Distribution for Measurement 3: Left: 125 DOFs, Right: Target

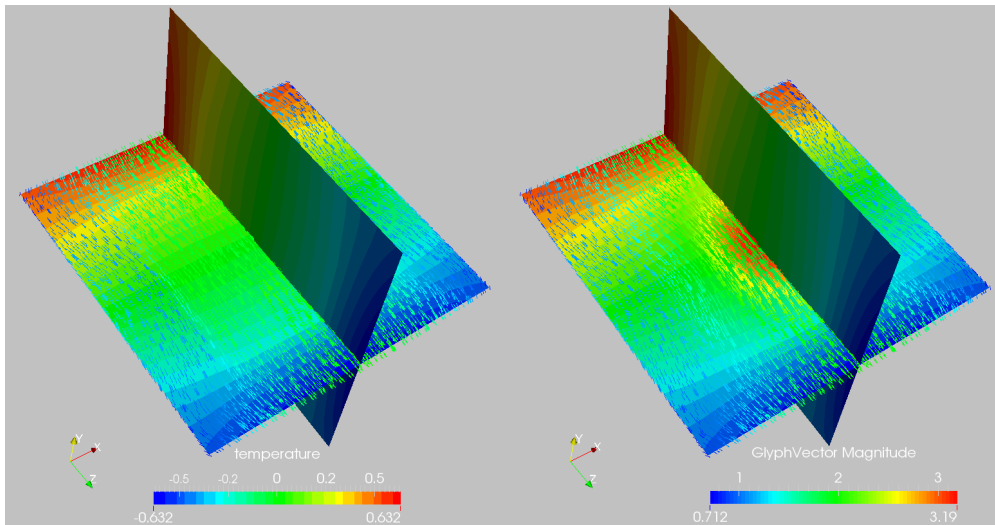


FIGURE 20. Cube - Gaussian k : Flux Distribution for Measurement 3: Left: 125 DOFs, Right: Target

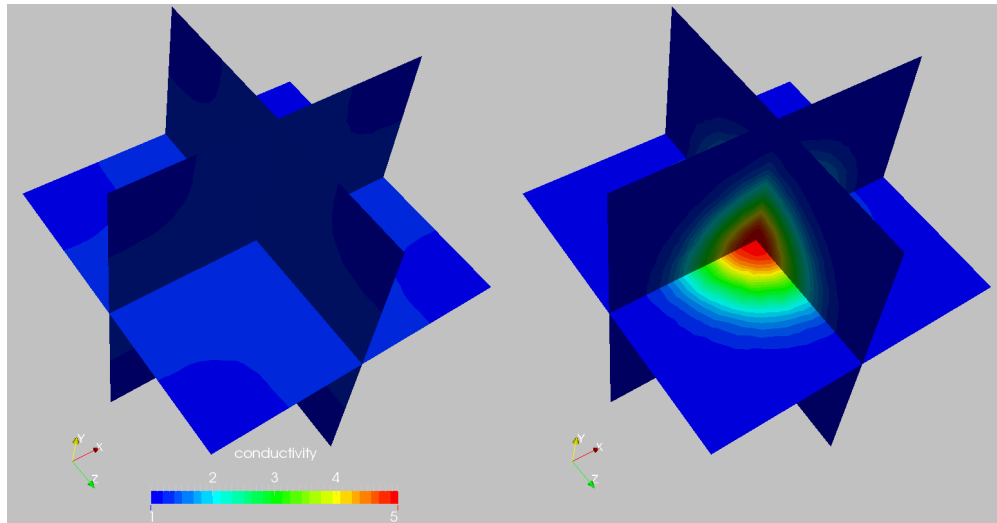


FIGURE 21. Cube - Gaussian k : Conductivity Distribution: Left: 250K DOFs, Right: Target

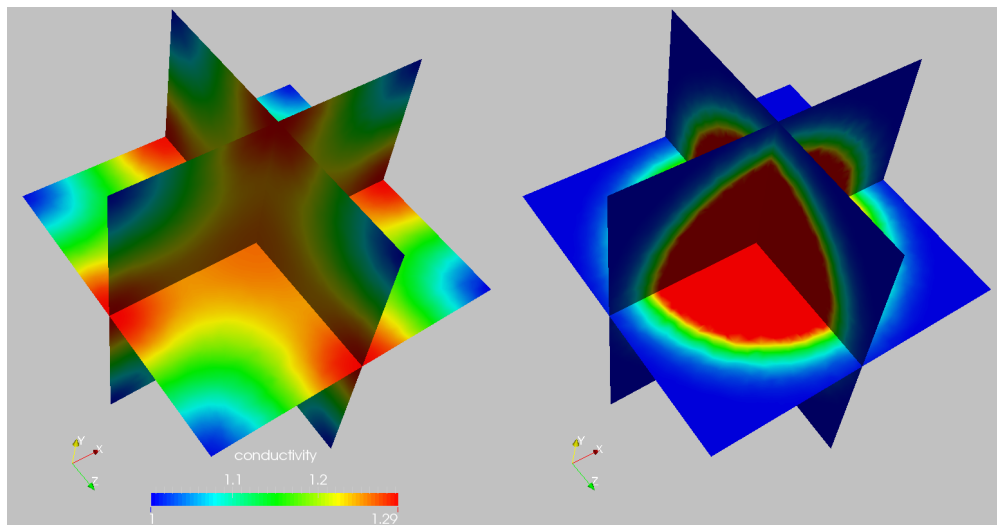


FIGURE 22. Cube - Gaussian k : Conductivity Distribution: Left: 250K DOFs, Right: Target (Note: Re-Scaled for Visualization)

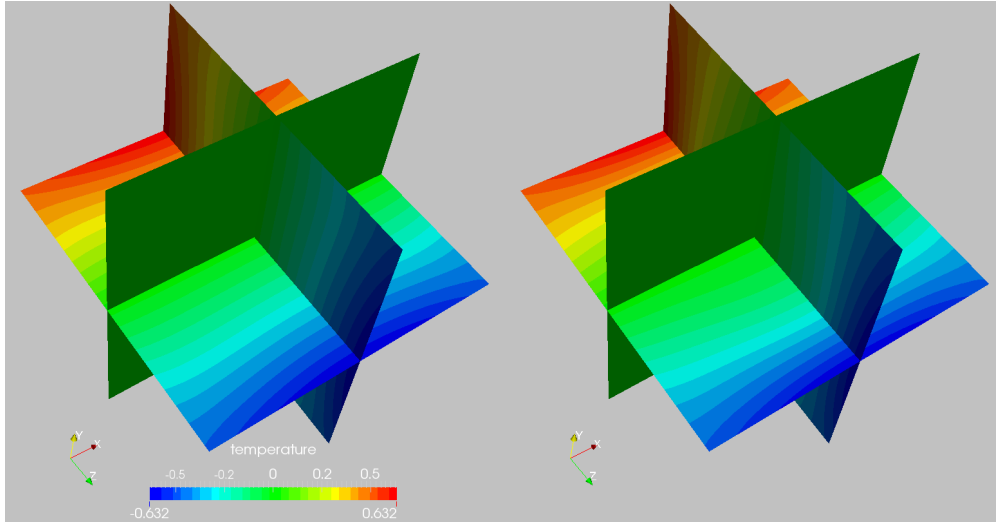


FIGURE 23. Cube - Gaussian k : Temperature Distribution for Measurement 3: Left: 250K DOFs, Right: Target

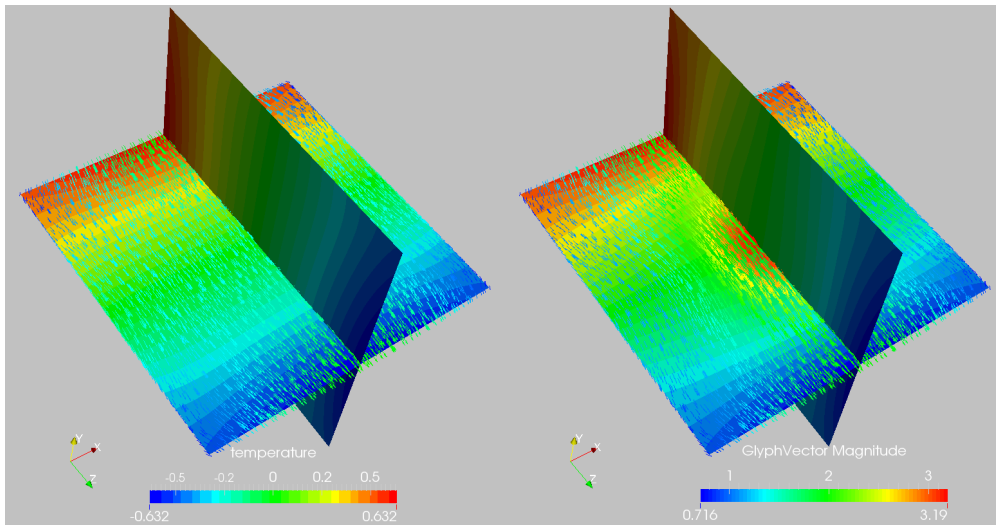


FIGURE 24. Cube - Gaussian k : Flux Distribution for Measurement 3: Left: 250K DOFs, Right: Target

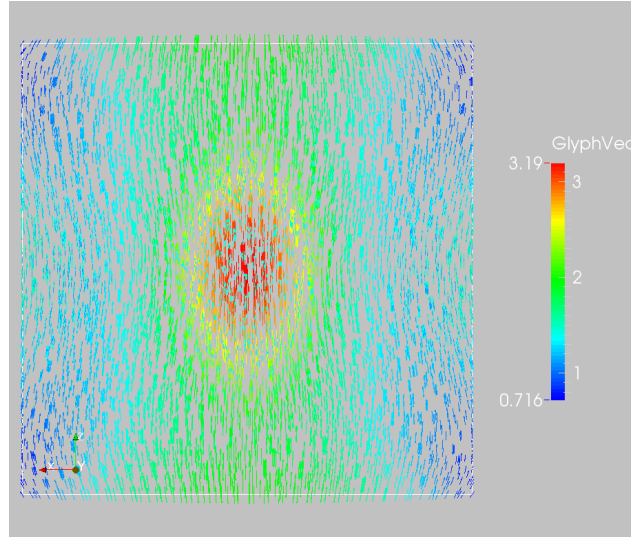


FIGURE 25. Cube - Gaussian k : Comparison of Fluxes for Plane $y = 0$

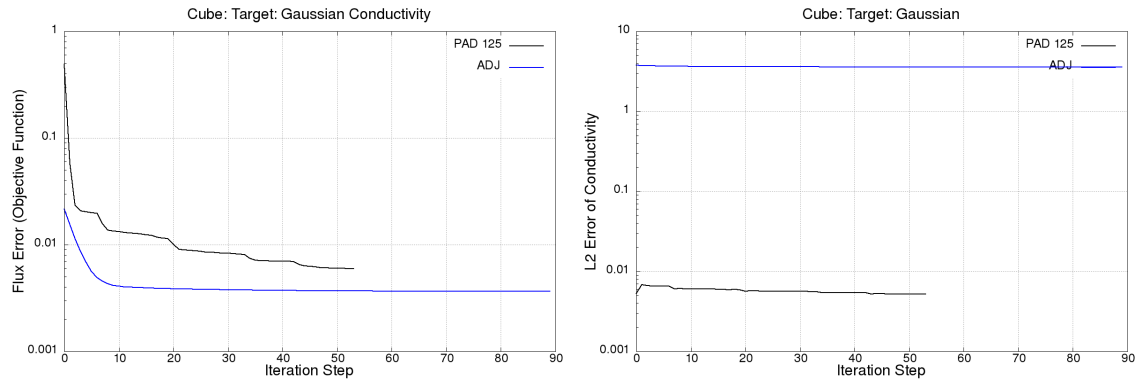


FIGURE 26. Cube - Gaussian k : Errors in Fluxes (left) and Conductivity (right).

8. CONCLUSIONS AND OUTLOOK

A finite element code for heat conduction, together with an adjoint solver and a suite of optimization tools were applied for the solution of Calderon's problem. One of the questions whose answer was sought was whether the solution to these problems is unique and obtainable. The results to date show that while the optimization procedure is able to obtain spatial distributions of the conductivity k that reduce the cost function significantly, the resulting conductivity k is still significantly different from the target distribution sought, particularly if a single temperature and flux field (i.e. 'measurement') is considered. While the normal fluxes recovered are very close to the prescribed ones, the tangential fluxes can differ considerably. As a possible way to circumvent these difficulties the prescription of several temperature and flux fields (i.e. 'measurements') at the same time were explored. The aim was to have as many boundary regions as possible with significant normal fluxes. The observation made here is that this technique yielded closer spatial distributions of the conductivity k to the targets desired, but that the effectiveness of number of 'measurements' tends to saturate at a relatively low number. For the cases run to date 2-4 measurements in 2-D and 3-6 measurements in 3-D seemed to give the best results.

At this point, it is not clear why rigorous mathematical proofs yield results of convergence and uniqueness, while in practice accurate distributions of the conductivity k seem to be elusive. One possible explanation is that the spatial influence of conductivities decreases exponentially with distance. Thus, many different conductivities inside a domain could give rise to very similar (infinitely close) boundary measurements.

REFERENCES

- [1] G. Alessandrini. Stable determination of conductivity by boundary measurements. *Appl. Anal.*, 27(1-3):153–172, 1988.
- [2] G. Alessandrini. Singular solutions of elliptic equations and the determination of conductivity by boundary measurements. *J. Differential Equations*, 84(2):252–272, 1990.
- [3] R.M. Brown and G.A. Uhlmann. Uniqueness in the inverse conductivity problem for nonsmooth conductivities in two dimensions. *Comm. Partial Differential Equations*, 22(5-6):1009–1027, 1997.
- [4] A.-P. Calderón. On an inverse boundary value problem. In *Seminar on Numerical Analysis and its Applications to Continuum Physics (Rio de Janeiro, 1980)*, pages 65–73. Soc. Brasil. Mat., Rio de Janeiro, 1980.
- [5] Z.Q. Chen. Reconstruction algorithms for electrical impedance tomography. *PhD Thesis Univ. of Wollongong (1990)*, 1990. <http://ro.uow.edu.au/theses/1348>.
- [6] M. Cheney, D. Isaacson, and J.C. Newell. Electrical impedance tomography. *SIAM Rev.*, 41(1):85–101, 1999.
- [7] V. Chitturi and N. Farrukh. Spatial resolution in electrical impedance tomography: A topical review. *Journal of Electrical Bioimpedance*, 8(1):66–78, 2019.
- [8] J. Feldman, M. Salo, and G. Uhlmann. Calderón problem: An introduction to inverse problems. *Preliminary notes on the book in preparation*, 2019.
- [9] R. Harikumar, R. Prabu, and S. Raghavan. Electrical impedance tomography (eit) and its medical applications: a review. *Int. J. Soft Comput. Eng.*, 3(4):193–198, 2013.
- [10] B. Harrach and J. Rieger. A set optimization technique for domain reconstruction from single-measurement electrical impedance tomography data. In *2017 MATRIX annals*, volume 2 of *MATRIX Book Ser.*, pages 37–49. Springer, Cham, 2019.
- [11] D. Isaacson. Distinguishability of conductivities by electric current computed tomography. *IEEE transactions on medical imaging*, 5(2):91–95, 1986.

- [12] R.V. Kohn and A. McKenney. Numerical implementation of a variational method for electrical impedance tomography. *Inverse Problems*, 6(3):389–414, 1990.
- [13] I.B. Lee. Determining conductivity by boundary measurements: some numerical results. Technical report, TN BN-1076. Institute for Physical Science and Technology, University of Maryland, 1988.
- [14] R. Löhner. *Applied computational fluid dynamics techniques: an introduction based on finite element methods*. John Wiley & Sons, 2008.

CENTER FOR COMPUTATIONAL FLUID DYNAMICS, COLLEGE OF SCIENCE, GEORGE MASON UNIVERSITY, FAIRFAX, VA 22030-4444, USA.

E-mail address: rlohner@gmu.edu

DEPARTMENT OF MATHEMATICAL SCIENCES, GEORGE MASON UNIVERSITY, FAIRFAX, VA 22030, USA.

E-mail address: hantil@gmu.edu